Stability of the Repulsive Fermi Gas with Contact Interactions

Yunpeng Ji, Grant L. Schumacher, Gabriel G. T. Assumpção, Jianyi Chen, Jere T. Mäkinen, Franklin J. Vivanco, and Nir Navon

Phys. Rev. Lett. **129**, 203402 — Published 10 November 2022

DOI: 10.1103/PhysRevLett.129.203402

Stability of the Repulsive Fermi Gas with Contact Interactions

Yunpeng Ji*,[1] Grant L. Schumacher,[1] Gabriel G. T. Assumpção,[1]
Jianyi Chen,[1] Jere Mäkinen,[1,2] Franklin J. Vivanco,[1] and Nir Navon[1,2]

[1]*Department of Physics, Yale University, New Haven, Connecticut 06520, USA*
[2]*Yale Quantum Institute, Yale University, New Haven, Connecticut 06520, USA*

(Dated: August 31, 2022)

We report the creation and the study of the stability of a repulsive quasi-homogeneous spin-$1/2$ Fermi gas with contact interactions. For the range of scattering lengths a explored, the dominant mechanism of decay is a universal three-body recombination towards a Feshbach bound state. We observe that the recombination coefficient $K_3 \propto \epsilon_{\rm kin} a^6$, where the first factor, the average kinetic energy per particle $\epsilon_{\rm kin}$, arises from a three-body threshold law, and the second one from the universality of recombination. Both scaling laws are consequences of Pauli blocking effects in three-body collisions involving two identical fermions. As a result of the interplay between Fermi statistics and the momentum dependence of the recombination process, the system exhibits non-trivial temperature dynamics during recombination, alternatively heating or cooling depending on its initial quantum degeneracy. The measurement of K_3 provides an upper bound for the interaction strength achievable in equilibrium for a uniform repulsive Fermi gas.

Repulsive interactions in Fermi systems are at the heart of some of the most interesting phenomena in quantum many-body physics. For instance, the interplay between the spin and orbital degrees of freedom gives rise to Stoner's itinerant ferromagnetism in the continuum [1] and to the complex phases of the repulsive Hubbard model on a lattice [2].

The dilute repulsive spin-1/2 Fermi gas, where the interactions between two spin states $\uparrow$ and $\downarrow$ are described by a positive s-wave scattering length a, is one of the most fundamental quantum many-body models [3–5]. Among its important features, it is amenable to first-principle calculations in perturbation (for $k_{\rm F}a \ll 1$, where $k_{\rm F}$ is the Fermi wavenumber). In that limit, its properties (e.g. ground-state energy, Landau parameters, etc.) are universal, i.e. they depend on a alone, not on details of short-range physics [5–7].

Ultracold atomic gases have emerged as a powerful platform for studying this model, because effective repulsion can be implemented on the so-called 'upper' (repulsive) branch using short-range attractive potentials [8–14]. This implementation is particularly interesting because it can realize the regime of strong ($k_{\rm F}a \gtrsim 1$) yet short-range ($k_{\rm F}r_0 \ll 1$, where r_0 is the potential range) interactions, see e.g. [15, 16].

However, the repulsive Fermi gas with short-range attractive potentials is intrinsically metastable. This originates from the existence of a universal bound state in the two-body problem for $a > 0$, with a binding energy $\epsilon_{\rm b} = \frac{\hbar^2}{ma^2}$ where m is the mass of the fermion. The pairing instability of the repulsive branch of the many-body system towards the lower (attractive) branch of bound pairs, depicted in Fig. 1(a), is a complex problem; it is expected to evolve from an instability driven by *universal* three-body recombination for $\epsilon_{\rm b} \gg E_{\rm F}$ [17, 18], to many-body pairing effects when $\epsilon_{\rm b} \lesssim E_{\rm F}$ [13, 17, 19, 20] where $E_{\rm F}$ is the Fermi energy.

This pairing instability has played a central role in the study of the strongly repulsive Fermi gas and the search for the itinerant-ferromagnet phase [16, 20–33]. Pioneering experiments have shown decreased lifetime of the gas with increasing interactions [8, 9] and larger initial rate of reduction of repulsive correlations (possibly due to the ferromagnetic instability) compared to the initial pairing rate [13, 14].

However, complex dynamics arising from the in-trap density inhomogeneity as well as the far-from-equilibrium nature of the initial quenched states have hindered the study of the homogeneous system's stability [8, 13]. The advent of homogeneous gases prepared in optical box traps [34–37] has enabled the investigation of complex stability problems in clean settings [38–40]. Here, we revisit the fundamental problem of the stability of the repulsive Fermi gas by measuring the three-body recombination law in a homogeneous atomic gas.

The experiment starts with a weakly attractive gas of ^{6}Li atoms in a balanced mixture of the first and third lowest Zeeman sublevels (respectively labeled as $\uparrow$ and $\downarrow$), trapped in a red-detuned optical dipole trap. The gas is evaporatively cooled at a bias magnetic field $B = 287$ G. It is then loaded in a blue-detuned (at a wavelength of 639 nm) cylindrical box trap constructed by intersecting a 'tube' beam (produced with a set of axicons) with two thin sheets, see Fig. 1(b). The magnetic field is then ramped to $B = 597$ G where the interactions are weakly repulsive ($a \approx 500\, a_0$, where a_0 is the Bohr radius [41]). At this stage, we typically have $N_\uparrow \approx N_\downarrow \approx 6 \times 10^5$ atoms per spin state at $T \approx 0.3\, T_{\rm F}$ with $E_{\rm F} \approx k_{\rm B} \times 0.5\ \mu$K and a spin imbalance of $\frac{N_\downarrow - N_\uparrow}{N_\downarrow + N_\uparrow} = 0.2(3)\%$. The interaction field is then ramped to its final value over 100 ms, and left to settle for an additional 25 ms. We then hold the atoms for a variable duration $t_{\rm hold}$. We image the gas near the zero crossing of a ($|a| \leq 50\ a_0$) by quickly ramping the field to $B = 569$ G, so that trapped pairs are converted into tightly bound molecules and thus detuned from the atomic imaging resonance [42, 43].

We show in Fig. 2(a) examples of time evolution of the atom number N per spin state for different values of a, normalized to the initial atom number N_0. Qualitatively, the gas lifetime decreases with increasing a, even though N_0 also decreases (because of losses during the interaction field ramp and the settling time [43]). The average kinetic energy per particle $\epsilon_{\rm kin}$, measured after time-of-flight expansion and shown in Fig. 2(b), also slowly decreases with $t_{\rm hold}$.

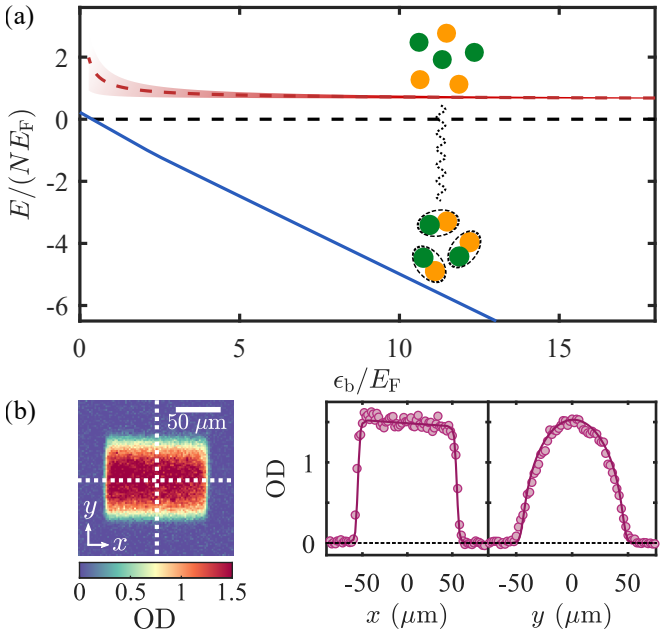

FIG. 1. A homogeneous repulsive Fermi gas prepared in an optical box. (a) Sketch of the two lowest energy branches of a Fermi gas with a positive scattering length a; the 'upper' (repulsive) branch is shown in red, the 'lower' branch (a gas of fermion pairs) is shown in blue. The red dashed line is the repulsive Fermi gas energy up to second order in $k_F a$ [3, 4]; the red shaded area depicts the energy width associated with the finite lifetime of the upper branch. (b) *In-situ* imaging of the box-trapped Fermi gas. Gravity, here oriented along $-\hat{\mathbf{y}}$, is compensated by magnetic levitation. The image on the left is the column-integrated optical density (OD). The plots on the right are cuts along the white dashed lines of the image. The solid lines are derived from the fit used to extract the volume of the box; $V = 7.3(6) \times 10^{-4}$ mm^3. The slanted profile in the horizontal cut is caused by the slightly conical shape of our cylindrical box [43].

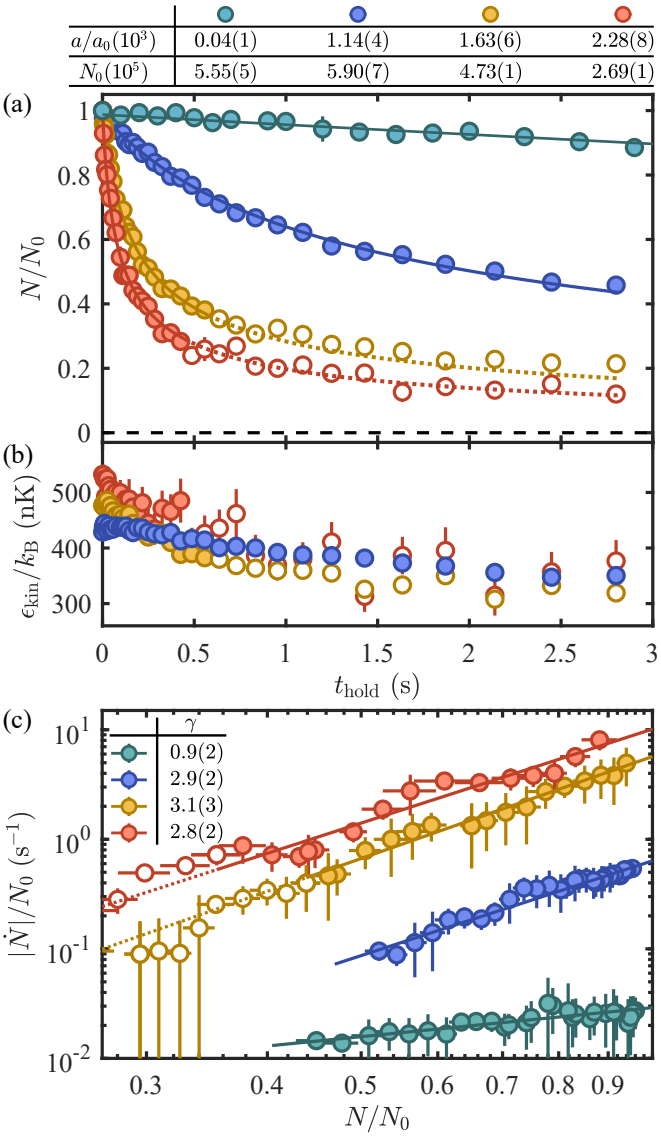

FIG. 2. Decay of a uniform repulsive Fermi gas. (a) Evolution of atom numbers for different interaction strengths, normalized to the initial atom numbers N_0. The solid blue, yellow, and red lines are fits to a three-body loss model that includes a one-body loss rate determined from the green-line fit [44]. The three-body loss fits are limited to the region where ϵ_{kin} changes by less than 20% of its initial value, indicated by solid circles; open circles are not used in the fit. The same marker style is used in (b) and (c). Dotted lines are extensions of the fits beyond the fitting range. (b) Evolution of the average kinetic energy per particle during atom losses. (c) Scaling relation between atom loss rate and atom number. Solid lines are power law fits and the extracted exponents γ are listed in the legend.

The origin of the decay is model-independently revealed by plotting the atom loss rate $\dot{N}/N_0$ versus N/N_0 (Fig. 2(c)). The examples shown follow a scaling relation of the rate $\dot{N} \propto -N^\gamma$ (fits are shown as solid lines, and fitted values of γ are in legend). We observe that $\gamma \approx 1$ at weak interactions ($a \ll 10^3\ a_0$) where the losses are caused by density-independent collisions with the residual background gas. For stronger interactions, we observe $\gamma \approx 3$, consistent with an atom loss rate per unit volume

$$\dot{n} = -L_3 n^3 \tag{1}$$

due to three-body collisions, with a constant loss coefficient L_3 and a uniform density $n = N/V$, where V is the volume of the box.

Now that we have established a range over which losses are dominated by three-body recombination, we quantitatively characterize the process. The event rate per unit volume for each type of event is $\Omega \equiv K_3 n^3$ ($= \Omega_{\uparrow\uparrow\downarrow} = \Omega_{\uparrow\downarrow\downarrow}$) where K_3 is the recombination coefficient; K_3 can be studied through losses, since $K_3 = L_3/d$, where d is the average number of atoms lost per event (either because their release energy from recombination exceeds the trap depth or because they form molecules that are optically detuned). We obtain L_3 by fitting $N(t)$ to the solution of Eq. (1) [44] (solid lines in Fig. 2(a)). To ensure that L_3 is approximately constant with t_{hold}, the fits are restricted to a range where ϵ_{kin} changes by at most 20% of the initial value, see solid points in Fig. 2 (the consistency of this analysis is discussed in [43]).

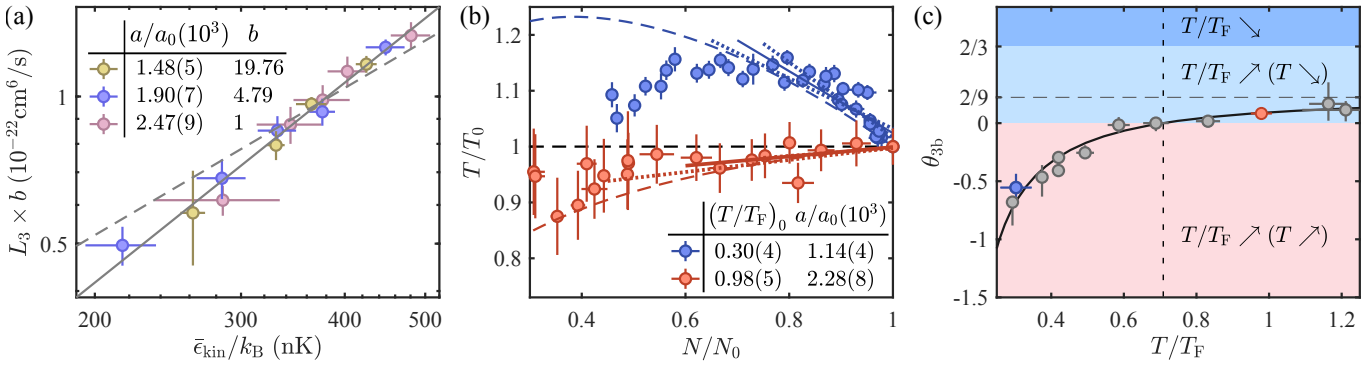

FIG. 3. Threshold law for the recombination of three spin-1/2 fermions. (a) Scaling relation between L_3 and the (time-averaged) kinetic energy $\bar{\epsilon}_{\rm kin}$. All three data sets are fitted with a common exponent $\lambda_{\rm exp}$ and with independent prefactors. For visual clarity, the data sets are rescaled by factors b (see legend) so that the power law fits are a single line (solid line). The dashed line is the fit assuming $\lambda = 1$ [43]. (b) Temperature evolution during three-body losses. The dashed lines are theoretical predictions without adjustable parameters, given the initial measured $(T/T_{\rm F})_0$ (see legend). The solid lines are linear fits to extract $\theta_{\rm 3b}$; the dotted lines show estimates on the uncertainties on $\theta_{\rm 3b}$, see panel (c). (c) Temperature-change coefficient $\theta_{\rm 3b}$ versus $T/T_{\rm F}$. The solid line is the theoretical prediction [43]. The vertical dashed line marks the critical $(T/T_{\rm F})^*$ at which $\theta_{\rm 3b}$ changes sign, and the horizontal dashed line shows the asymptotic value of $\theta_{\rm 3b}$ in the classical limit.

We examine this assumption more carefully by studying the relationship between L_3 and $\epsilon_{\rm kin}$. We control $\epsilon_{\rm kin}$ by varying the box depth at an intermediate evaporative cooling stage, keeping the final box depth $U_{\rm box}$ the same. As shown in Fig. 3(a) for three different values of a, we observe that L_3 scales as a power law of $\epsilon_{\rm kin}$ averaged over time, $\bar{\epsilon}_{\rm kin}$.

Theoretically, $K_3 \propto \epsilon_{\rm kin}^{\lambda}$, where the exponent λ is determined by the three-body threshold laws, which crucially depends on the symmetries imposed by the quantum statistics of the collision participants [18]. For instance, for three distinguishable particles or indistinguishable bosons, there is no energy dependence ($\lambda = 0$); for three indistinguishable fermions, $\lambda = 2$ [45, 46]. The generic process in the spin-1/2 Fermi gas corresponds to the previously-unverified case of collisions involving two indistiguishable fermions. The three-body event rate in a unit volume ω_3 depends on the momenta $\mathbf{k}_1$ and $\mathbf{k}_2$ of the indistinguishable fermions, and is independent of the third participant's momentum $\mathbf{k}'$ [47]:

$$\omega_3(\mathbf{k}_1, \mathbf{k}_2, \mathbf{k}') \propto (\mathbf{k}_1 - \mathbf{k}_2)^2. \qquad (2)$$

Integrating Eq. (2) over the phase space density of the three participants, one finds $\lambda = 1$. Experimentally, we measure $\lambda_{\rm exp} = 1.36(14)$ [48] (solid line in Fig. 3(a)), in reasonable agreement with the theoretical prediction.

The dependence of ω_3 on momentum has interesting implications on the temperature dynamics of the gas during decay. In Fig. 3(b), we show T/T_0 versus N/N_0 (where T_0 is the initial T). Depending on $T/T_{\rm F}$, the system either cools down or heats up. This effect results from an interplay between Fermi correlations and the momentum dependence of ω_3. The cooling effect from the preferential removal of particles with large momenta (without spatial selectivity) [43], strongest for $T \gg T_{\rm F}$, competes with the heating from the perforation of the Fermi sea, which dominates in the deeply degenerate regime [49]. A theoretical model describing this interplay, shown as colored dashed lines in Fig. 3(b), yields good agreement with the observed evolution of the temperature for $N/N_0 \gtrsim 0.7$ [43]. The discrepancy at late times for low $(T/T_{\rm F})_0$ might be due to additional cooling from plain evaporation.

Quantitatively, we define the coefficient $\theta_{\rm 3b} \equiv \frac{N}{T}\left(\frac{\partial T}{\partial N}\right)_V$ under this rarefaction [43], and measure it at $t_{\rm hold} = 0$ for various $T/T_{\rm F}$ (Figs. 3(b)-(c)). We observe that the transition from heating to cooling occurs at a critical degeneracy $(T/T_{\rm F})^* \approx 0.7$. The measurements are in excellent agreement with the theoretical prediction (solid line in Fig. 3(c)) [43], which establishes the crossing at $(T/T_{\rm F})^* = 0.71$ (vertical dashed line). It is worthwhile to note that $\theta_{\rm 3b}$ - and consequently $(T/T_{\rm F})^*$ - is governed only by the momentum dependence of ω_3 (Eq. (2)); it is independent of the a-dependent prefactor of ω_3 [43]. For $T \gg T_{\rm F}$, $\theta_{\rm 3b}$ approaches $2/9$, where the cooling effect is most pronounced. Note that for all T, $\theta_{\rm 3b} < 2/3$, so that this process does not increase the quantum degeneracy of the gas (see related scenarios for bosons [50, 51], and fermions near a narrow Feshbach resonance [52]).

We now turn to the dependence of L_3 on interactions. In Fig. 4(a), we display γ versus a; the solid points are data where losses are three-body dominated (see Fig. 4 and caption). We subsequently extract L_3 for all interactions by fixing $\gamma = 3$ and taking one-body decay into account [44]; to factor out the effect of the threshold law, we display $L_3/\bar{\epsilon}_{\rm kin}$, see Fig. 4(b). We observe that over more than four orders of magnitude, $L_3/\bar{\epsilon}_{\rm kin}$ follows a power law of a. Fitting the data in the three-body-dominated region (solid blue points in Fig. 4(b)), we find $L_3/\bar{\epsilon}_{\rm kin} \propto a^{6.1(2)}$ (solid blue line).

The fact that L_3 scales precisely as a^6 is strong evidence for the universality of this process. Indeed, should three-body recombination be universal, i.e. be independent of short-range physics, the threshold law implies the scaling of K_3 with interaction strength [53]. Specifically, if $K_3 \propto \epsilon_{\rm kin}^{\lambda}$, then on

dimensional grounds, $K_3 \propto \epsilon_{\rm kin}^{\lambda} \frac{m^{\lambda-1}}{\hbar^{2\lambda-1}} a^{4+2\lambda}$. For two identical fermions, one finds $K_3 \propto a^6$, in excellent agreement with our measurements. Compared to the bosonic case, where $K_3 \propto a^4$ [54–56], an additional factor $\epsilon_{\rm kin}/\epsilon_{\rm b}$, $\propto (k_{\rm F}a)^2$ at low T, can be interpreted as a suppression factor due to Pauli blocking, which arises as two identical fermions need to come within $\approx a$ of each other to form a final bound state.

Now that we established $L_3 \propto \epsilon_{\rm kin} a^6$, we can extract the dimensionless constant A in $L_3 = dA\epsilon_{\rm kin} a^6/\hbar$, predicted to be universal. As some or all products of the recombination can be lost, d, the link between losses and recombinations, depends on the box depth $U_{\rm box}$ and $\epsilon_{\rm b}$. To gain insight into this link, we implement a second imaging protocol where we image the atoms directly at the interaction field (see label '4B' in the top left inset of Fig. 4(b)); in our range of a, molecules and atoms are optically unresolved [42]. The measurements are displayed as red circles in Figs. 4(a)-(b).

At low a, L_3 measured by both imaging methods coincide, as $d = 3$ in both cases. The separation at $a \gtrsim 1300\ a_0$ occurs close to the condition $\epsilon_{\rm b}/3 \approx 2U_{\rm box}$ at which the molecules remain trapped (see cartoons at the bottom of Fig. 4(b)) [57]. For larger a, $d < 3$ for the 'interaction field' imaging.

For the 'zero-crossing' imaging (see label '4A' in the top left inset of Fig. 4(b)), $d = 3$ still holds; the a^6 scaling extends up to the point where $2\epsilon_{\rm b}/3 < U_{\rm box}$, beyond which all recombination products may be trapped [17, 58, 59]. The maximum of $L_3(a)$ is located marginally beyond this threshold. Fixing $d = 3$, we fit $L_3/\bar{\epsilon}_{\rm kin}$ (solid blue points) and find $A = 143(16)_{\rm stat.}(24)_{\rm sys.}$. To examine more closely the quality of the a^6 scaling, we extract A without free parameters from $(\hbar L_3/(3\bar{\epsilon}_{\rm kin}))/a^6$ (Fig. 4(c)). Our measurements are in excellent agreement with the theoretical prediction $A = 148$ for the mass-balanced three-fermion problem [17].

The range over which the a^6 scaling law applies is surprisingly large. First, it extends even at large a where the measured γ is only marginally close to 3 (see open circles in Fig. 4). Secondly, at the highest a for which we observe a^6 scaling, $\epsilon_{\rm kin} \gtrsim k_{\rm B} \times 0.5\ \mu$K is only slightly smaller than $\epsilon_{\rm b} \approx k_{\rm B} \times 1.2\ \mu$K, even though the condition for the universal scaling is expected to be valid for $\epsilon_{\rm kin} \ll \epsilon_{\rm b}$ [17].

Finally, our measurement of K_3 provides an important ingredient for assessing the limits of equilibrium for a strongly interacting repulsive Fermi gas. To ensure equilibrium, $\Gamma_3 \equiv 3K_3 n^2$ [60] must be significantly smaller than Γ_2, the two-body elastic collision rate. The largest interaction strength for which $\Gamma_2 = \Gamma_3$ is $k_{\rm F}a \approx 1.0$, and it is reached for $T \approx 0.85\ T_{\rm F}$ [61, 66]. This limit is close to the predicted point for the ferromagnetic transition, $k_{\rm F}a = \pi/2$ in the mean-field approximation [67] and ≈ 1 in quantum Monte Carlo simulations [20, 28, 30].

In conclusion, we studied the stability of the repulsive Fermi gas with short-range interactions. We measured the universal recombination law for three particles of equal mass involving two identical fermions. This work paves the way for the study of complex stability problems of Fermi systems in clean uniform settings, e.g. multi-component gases [68–70], mass-imbalanced mixtures [71–75], and molecules [76, 77]. A future work could leverage uniform Fermi gases to explore the regime $\epsilon_{\rm b} \lesssim \epsilon_{\rm kin}$, where $K_3 \propto \epsilon_{\rm kin} a^6$ should no longer hold; in that regime, many-body pairing mechanisms are expected to take over at low temperature [19, 20]. To access the shorter time scales expected, fast state preparation and probing techniques such as internal state manipulation could be useful [13, 14].

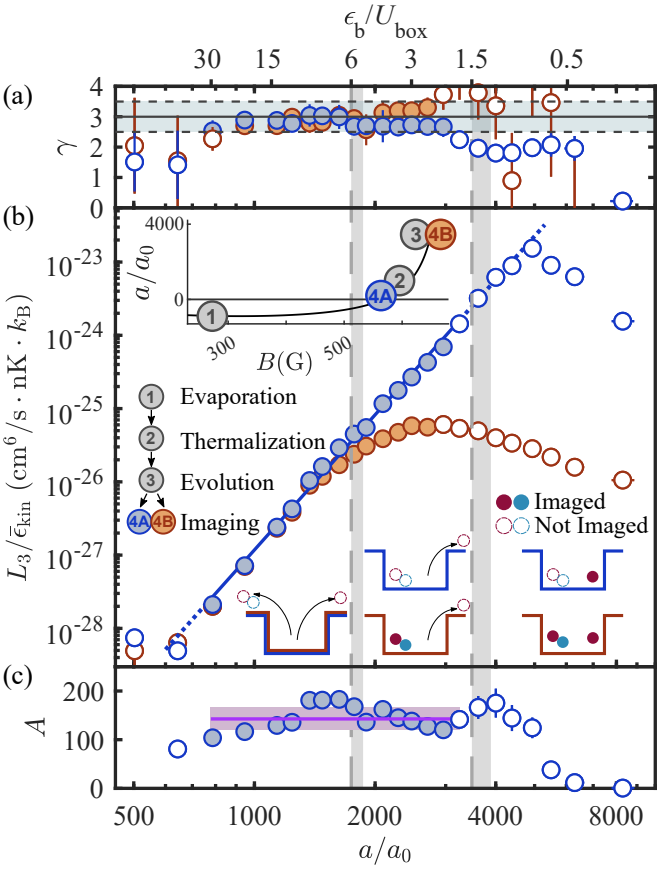

FIG. 4. Universality of three-body recombination. (a) Atom-loss scaling exponent γ. Blue and red circles are respectively imaged near the zero crossing of a or directly at the interaction field. Data in the three-body dominant region, selected by $|\gamma - 3| \leq 0.5$ (blue band) and with a relative uncertainty $\leq 20\%$, are shown by solid points and left open otherwise, in all panels. (b) Universal scaling of L_3 with a. The experiment sequence is shown in the upper insets. The blue line is the power law fit to the solid blue points. Vertical grey dashed lines mark the threshold values of a such that $\epsilon_{\rm b}/3 = 2U_{\rm box}$ and $2\epsilon_{\rm b}/3 = U_{\rm box}$, and the bands include average over initial energies [43]. Bottom cartoons depict imaging and trapping regimes after recombinations for the atoms and molecules. (c) Universal constant A. Data points are the experimental values of $A = \hbar L_3/(3\bar{\epsilon}_{\rm kin} a^6)$, and the solid purple line is derived from a global a^6 fit to the data in (b) (not shown). The systematic error from the volume calibration is shown by the light purple band [43].

We thank D.S. Petrov, F. Scazza, M. Zaccanti, G. Roati, and O. Goulko for fruitful discussions. We also thank Z. Hadzibabic, F. Werner, S. Huang and L. Chambard for comments on the manuscript. This work was supported by the

NSF (Grant Nos. PHY-1945324 and PHY-2110303), DARPA (Grant No. W911NF2010090), the David and Lucile Packard Foundation, and the Alfred P. Sloan Foundation. G.L.S acknowledges support from the NSF Graduate Research Fellowship Program. J.M. acknowledges support from the Yale Quantum Institute.

* To whom correspondence should be addressed: yunpeng.ji@yale.edu.

[1] E. C. Stoner, Lond. Edinb. Dubl. Phil. Mag. **15**, 1018 (1933).
[2] A. Mielke and H. Tasaki, Commun. Math. Phys. **158**, 341 (1993).
[3] K. Huang and C. N. Yang, Phys. Rev. **105**, 767 (1957).
[4] T. Lee and C. Yang, Phys. Rev. **105**, 1119 (1957).
[5] V. M. Galitskii, Sov. Phys. JETP. **3**, 104 (1958).
[6] L. D. Landau, Sov. Phys. JETP. **5**, 101 (1957).
[7] D. V. Efremov, M. S. Mar'enko, M. A. Baranov, and M. Y. Kagan, J. Exp. Theor. Phys. **90**, 861-871 (2000).
[8] G.-B. Jo, Y.-R. Lee, J.-H. Choi, C. A. Christensen, T. H. Kim, J. H. Thywissen, D. E. Pritchard, and W. Ketterle, Science **325**, 1521-1524 (2009).
[9] C. Sanner, E. J. Su, W. Huang, A. Keshet, J. Gillen, and W. Ketterle, Phys. Rev. Lett. **108**, 240404 (2012).
[10] Y.-R. Lee, M.-S. Heo, J.-H. Choi, T. T. Wang, C. A. Christensen, T. M. Rvachov, and W. Ketterle, Phys. Rev. A **85**, 063615 (2012).
[11] G. Valtolina, F. Scazza, A. Amico, A. Burchianti, A. Recati, T. Enss, M. Inguscio, M. Zaccanti, and G. Roati, Nat. Phys. **13**, 704-709 (2017).
[12] F. Scazza, G. Valtolina, P. Massignan, A. Recati, A. Amico, A. Burchianti, C. Fort, M. Inguscio, M. Zaccanti, and G. Roati, Phys. Rev. Lett. **118**, 083602 (2017).
[13] A. Amico, F. Scazza, G. Valtolina, P. Tavares, W. Ketterle, M. Inguscio, G. Roati, and M. Zaccanti, Phys. Rev. Lett. **121**, 253602 (2018).
[14] F. Scazza, G. Valtolina, A. Amico, P. E. S. Tavares, M. Inguscio, W. Ketterle, G. Roati, and M. Zaccanti, Phys. Rev. A **101**, 013603 (2020).
[15] L. Pricoupenko and Y. Castin, Phys. Rev. A **69**, 051601 (2004).
[16] V. B. Shenoy and T.-L. Ho, Phys. Rev. Lett. **107**, 210401 (2011).
[17] D. S. Petrov, Phys. Rev. A **67**, 010703 (2003).
[18] B. Esry, C. H. Greene, and H. Suno, Phys. Rev. A **65**, 010705 (2001).
[19] D. Pekker, M. Babadi, R. Sensarma, N. Zinner, L. Pollet, M. W. Zwierlein, and E. Demler, Phys. Rev. Lett. **106**, 1 (2011).
[20] L. He, X.-J. Liu, X.-G. Huang, and H. Hu, Phys. Rev. A **93**, 063629 (2016).
[21] R. A. Duine and A. H. MacDonald, Phys. Rev. Lett. **95**, 230403 (2005).
[22] L. LeBlanc, J. Thywissen, A. Burkov, and A. Paramekanti, Phys. Rev. A **80**, 013607 (2009).
[23] G. J. Conduit and E. Altman, Phys. Rev. A **83**, 043618 (2011).
[24] G. J. Conduit, A. G. Green, and B. D. Simons, Phys. Rev. Lett. **103**, 207201 (2009).
[25] G. J. Conduit and B. D. Simons, Phys. Rev. A **79**, 053606 (2009).
[26] C.-C. Chang, S. Zhang, and D. M. Ceperley, Phys. Rev. A **82**, 061603 (2010).
[27] R. Schmidt and T. Enss, Phys. Rev. A **83**, 063620 (2011).
[28] S. Pilati, G. Bertaina, S. Giorgini, and M. Troyer, Phys. Rev. Lett. **105**, 030405 (2010).
[29] C. W. von Keyserlingk and G. J. Conduit, Phys. Rev. A **83**, 053625 (2011).
[30] S.-Y. Chang, M. Randeria, and N. Trivedi, Proc. Natl. Acad. Sci. U.S.A. **108**, 51 (2011).
[31] P. Massignan, Z. Yu, and G. M. Bruun, Phys. Rev. Lett. **110**, 230401 (2013).
[32] S. Pilati, I. Zintchenko, and M. Troyer, Phys. Rev. Lett. **112**, 015301 (2014).
[33] I. Zintchenko, L. Wang, and M. Troyer, Eur. Phys. J. B **89**, 1 (2016).
[34] A. L. Gaunt, T. F. Schmidutz, I. Gotlibovych, R. P. Smith, and Z. Hadzibabic, Phys. Rev. Lett. **110**, 200406 (2013).
[35] L. Chomaz, L. Corman, T. Bienaimé, R. Desbuquois, C. Weitenberg, S. Nascimbene, J. Beugnon, and J. Dalibard, Nat. Commun. **6**, 1 (2015).
[36] B. Mukherjee, Z. Yan, P. B. Patel, Z. Hadzibabic, T. Yefsah, J. Struck, and M. W. Zwierlein, Phys. Rev. Lett. **118**, 123401 (2017).
[37] N. Navon, R. P. Smith, and Z. Hadzibabic, Nat. Phys. **17**, 1334 (2021).
[38] C. Eigen, J. A. Glidden, R. Lopes, N. Navon, Z. Hadzibabic, and R. P. Smith, Phys. Rev. Lett. **119**, 250404 (2017).
[39] R. Bause, A. Schindewolf, R. Tao, M. Duda, X.-Y. Chen, G. Quéméner, T. Karman, A. Christianen, I. Bloch, and X.-Y. Luo, Phys. Rev. Research **3**, 033013 (2021).
[40] C. Shkedrov, M. Menashes, G. Ness, A. Vainbaum, E. Altman, and Y. Sagi, Phys. Rev. X **12**, 011041 (2022).
[41] G. Zürn, T. Lompe, A. N. Wenz, S. Jochim, P. Julienne, and J. Hutson, Phys. Rev. Lett. **110**, 135301 (2013).
[42] $\epsilon_b = \hbar\Gamma$, where Γ is the natural linewidth of the imaging resonance, corresponds to $a \approx 300\ a_0$.
[43] See Supplemental Material.
[44] Including the effect of one-body losses in the equation for $\dot{n}$ yields: $\dot{n} = -L_3 n^3 - n/\tau_1$, where $\tau_1 = 32(2)$ s is the background-gas limited lifetime. This effect is small for all but the smallest a we explored.
[45] J. Yoshida, T. Saito, M. Waseem, K. Hattori, and T. Mukaiyama, Phys. Rev. Lett. **120**, 133401 (2018).
[46] F. Ç. Top, Y. Margalit, and W. Ketterle, Phys. Rev. A **104**, 043311 (2021).
[47] D. S. Petrov, private communication.
[48] The x-axis values in Fig.3(a) are the kinetic energies averaged over the range L_3 is extracted [43].
[49] E. Timmermans, Phys. Rev. Lett. **87**, 240403 (2001).
[50] M. Schemmer and I. Bouchoule, Phys. Rev. Lett. **121**, 200401 (2018).
[51] L. H. Dogra, J. A. Glidden, T. A. Hilker, C. Eigen, E. A. Cornell, R. P. Smith, and Z. Hadzibabic, Phys. Rev. Lett. **123**, 020405 (2019).
[52] S. Peng, H. Liu, J. Li, and L. Luo, (2021), arXiv:2107.07078.
[53] J. D'Incao and B. Esry, Phys. Rev. Lett. **94**, 213201 (2005).
[54] E. Braaten and H. W. Hammer, Ann. Phys. (N. Y.) **322**, 120 (2007).
[55] P. Naidon and S. Endo, Eur. Phys. J. B **80**, 056001 (2017).
[56] In reality, the universal a^4 scaling that one would expect for bosons is only approximate because the three-boson problem with two-body contact interactions is nonuniversal: it necessitates the addition of a three-body parameter. By contrast, the three-body problem involving two identical fermions, each of mass m, and a third atom of mass m', is universal provided $m/m' < 13.6$ [17].
[57] In retrospect, it is puzzling that the effect of the deposited en-

ergy of produced molecules is not seen, given that the atom-molecule scattering length $\approx a$ [78].
[58] S. Zhang and T.-L. Ho, New J. Phys. **13**, 055003 (2011).
[59] One can naively estimate the unitary limit of L_3 by substituting a with thermal wavelength $\lambda_T = h/\sqrt{2\pi m k_B T}$. For $T \approx 500$ nK, we find $L_3/\epsilon_{\rm kin} \approx 6 \times 10^{-20}$ cm^6/(s $\cdot$ nK $\cdot$ k_B), well above our highest $L_3/\bar{\epsilon}_{\rm kin}$.
[60] Depending on whether the third atom is trapped after a three-recombination event, $\Gamma_3/(K_3 n^2)$ is a number between 2 and 3. Here we consider the worst case scenario.
[61] See Supplemental Material for the calculation of Γ_2, which includes Refs. [62–65]
[62] E. M. Lifschitz and L. P. Pitaevskii, *Physical Kinetics* (Pergamon Press, Oxford, 1981).
[63] O. J. Luiten, M. W. Reynolds, and J. T. M. Walraven, Phys. Rev. A **53**, 381 (1996).
[64] M. E. Gehm, S. L. Hemmer, K. M. O'Hara, and J. Thomas, Phys. Rev. A **68**, 011603 (2003).
[65] T. Lepers, D. Davesne, S. Chiacchiera, and M. Urban, Phys. Rev. A **82**, 023609 (2010).
[66] Note that this limit is only marginally consistent, since it is calculated assuming the universal K_3 law; this assumption is expected to break down for $\epsilon_b \lesssim E_F$.
[67] M. Houbiers, R. Ferwerda, H. Stoof, W. McAlexander, C. Sackett, and R. Hulet, Phys. Rev. A **56**, 4864 (1997).
[68] T. B. Ottenstein, T. Lompe, M. Kohnen, A. N. Wenz, and S. Jochim, Phys. Rev. Lett. **101**, 203202 (2008).
[69] J. Huckans, J. Williams, E. Hazlett, R. Stites, and K. O'Hara, Phys. Rev. Lett. **102**, 165302 (2009).
[70] S. Nakajima, M. Horikoshi, T. Mukaiyama, P. Naidon, and M. Ueda, Phys. Rev. Lett. **105**, 023201 (2010).
[71] M. Taglieber, A.-C. Voigt, T. Aoki, T. Hänsch, and K. Dieckmann, Phys. Rev. Lett. **100**, 010401 (2008).
[72] E. Wille, F. Spiegelhalder, G. Kerner, D. Naik, A. Trenkwalder, G. Hendl, F. Schreck, R. Grimm, T. Tiecke, J. Walraven, *et al.*, Phys. Rev. Lett. **100**, 053201 (2008).
[73] G. Barontini, C. Weber, F. Rabatti, J. Catani, G. Thalhammer, M. Inguscio, and F. Minardi, Phys. Rev. Lett. **103**, 043201 (2009).
[74] R. Pires, J. Ulmanis, S. Häfner, M. Repp, A. Arias, E. Kuhnle, and M. Weidemüller, Phys. Rev. Lett. **112**, 250404 (2014).
[75] S.-K. Tung, K. Jimenez-Garcia, J. Johansen, C. V. Parker, and C. Chin, Phys. Rev. Lett. **113**, 240402 (2014).
[76] D. K. Hoffmann, T. Paintner, W. Limmer, D. S. Petrov, and J. H. Denschlag, Nat. Commun. **9**, 1 (2018).
[77] M. Duda, X.-Y. Chen, R. Bause, A. Schindewolf, I. Bloch, and X.-Y. Luo, (2022), arXiv:2202.06940.
[78] G. Skorniakov and K. Ter-Martirosian, Sov. Phys. JETP. **4** (1957).